LANGMUIR

Article

pubs.acs.org/Langmuir

Organization and Structure of Branched Amphipathic Oligopeptide Bilayers

Zhiguang Jia, Susan K. Whitaker, John M. Tomich, and Jianhan Chen*

Department of Biochemistry and Molecular Biophysics, Kansas State University, Manhattan, Kansas 66506, United States

Supporting Information

ABSTRACT: A class of self-assembling branched amphiphilic peptide capsules (BAPCs) was recently developed that could serve as a new drug delivery vehicle. BAPCs can encapsulate solutes up to ~12 kDa during assembly, are unusually stable, and are readily taken up by cells with low cytotoxicity. Coarse-grained simulations have supported that BAPCs are defined by bilayers that resemble those formed by diacyl phospholipids. Here, atomistic simulations were performed to characterize the structure and organization of bilayers formed by three branched amphiphilic peptides (BAPs): bis(Ac-FLIVIGSII)-K-K_4-CO-NH_2, bis(Ac-CHA-LIVIGSII)-K-K_4-CO-NH_2, and bis(Ac-FLIVI)-K-K_4-CO-NH_2. The results show BAPs form a network of intra- and intermolecular backbone hydrogen bonds within the same leaflet in addition to hydrophobic side-chain interactions. The terminal residues of two leaflets form an interdigitation region locking two leaflets together. The phenyl groups in bis(Ac-FLIVIGSII)-K-K_4-CO-NH_2 and bis(Ac-FLIVI)-K-K_4-CO-NH_2 are tightly packed near the bilayer center but do not formed ordered structures with specific $\pi-\pi$ stacking. Replacing phenyl groups with the cyclohexane side chain only slightly increases the level of disorder in bilayer structures and thus should not significantly affect the stability, consistent with experimental results on bis(Ac-CHA-LIVIGSII)-K-K_4-CO-NH_2 BAPCs. Self-assembly simulations further suggest that leaflet interdigitation likely occurs at early stages of BAPC formation. Atomistic simulations also reveal that the BAPC bilayers are highly permeable to water. This prediction was validated using fluorescence measurements of encapsulated self-quenching dye upon transferring BAPCs to buffers with different salt concentrations. Improved understanding of the organization and structure of BAPC bilayers at the atomic level will provide a basis for future rational modifications of BAP sequence to improve BAPC properties as a new class of delivery vehicle.

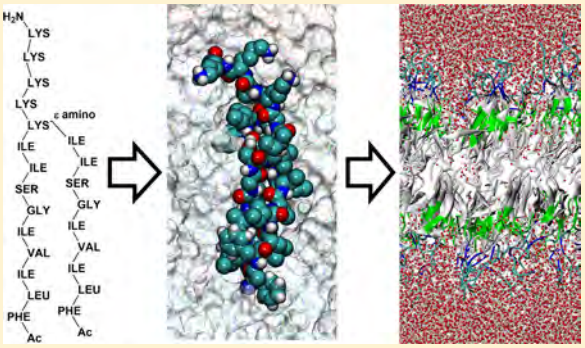

INTRODUCTION

The use of drugs in free forms are often limited by unfavorable properties such as low aqueous solubility, poor biodistribution, and high breakdown rate in vitro or in vivo.[1] In addition, some drugs are toxic or have potential danger of inducing an immune response when administered directly.[2,3] To compensate for these undesirable properties and improve therapeutic efficiency, association of drugs with appropriate drug carriers is often necessary.[1] However, while tremendous improvements have been made over the years, some important limitations remain for the currently available drug carriers.[1,3] For example, it remains challenging for lipid/polymeric-based vesicles to deliver drugs to specific organs or tissues, and uptake of drugs by off-target organs often leads to side effects.[2] It also remains difficult for traditional lipid-based carrier to deliver macromolecules such as protein or highly charged molecules such as oligonucleotides for siRNA and gene therapy.[2,4,5] In addition, intracellular degradation products of some polymeric-based carrier can be toxic.[3] As protein drugs and gene therapeutics become increasingly promising tools against diseases such as cancers, heritable genetic disorders, and viral infections, there is a pressing need to develop new drug delivery vehicles and overcome these shortcomings.[2,4,6]

Gudlur et al. first described a new peptide-based nanovesicle, formed from aqueous self-assembly of branched amphiphilic peptides (BAP).[7] The molecular architecture of BAPs was designed to mimic that of diacyl phospholipids. It contains a polylysine headgroup, analogous to the charged phosphate-based head of lipid, and two identical hydrophobic segments connected to α and ε amino groups of the N-terminal lysine residue. The chemical structures of three BAPs investigated in the current study—bis(Ac-FLIVIGSII)-K-K_4-CO-NH_2, bis(Ac-CHA-LIVIGSII)-K-K_4-CO-NH_2, and bis(Ac-FLIVI)-K-K_4-CO-NH_2 peptides—are shown in Figure 1. Coarse-grained (CG) simulations have demonstrated that BAPs can self-assemble into bilayers in water, in a manner similar to diacyl phospholipids.[7,8] The resulting BAP capsules (BAPCs) have diameters ranging from 20 nm to 2 μm depending on the assembly and annealing temperatures.[11] BAPCs have several

Received: June 29, 2016
Revised: August 30, 2016
Published: September 1, 2016

DOI: 10.1021/acs.langmuir.6b02421
Langmuir 2016, 32, 9883−9891

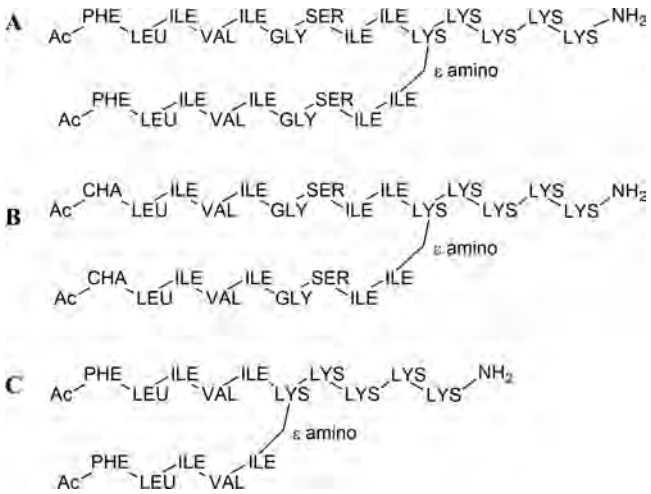

Figure 1. Schematic representations of three BAPs involved in this study.

attractive properties as a potential delivery vesicle. They can encapsulate macromolecules, up to ~12 kDa proteins, and have long intracellular lifetime (>2 weeks) after uptake.[8−10] BAPCs are extremely stable in water and can maintain their structure to at least 95 °C.[8] Although their high stability allows the BAPCs to be used to deliver radioisotopes for cancer therapy, it is difficult to use BAPCs as a general drug delivery system.[9] To design new BAP sequences with higher cargo release rate, improved knowledge of the organization and structure of BAP bilayers is necessary.

Circular dichroism (CD) spectra analysis shows that BAPs mainly sample a mixture of β and random coil secondary structures, and their conformational states can depend quite sensitively on the temperature of self-assembly and post-assembly annealing process. Specifically, the BAP assembled at 37 or 4 °C was found trapped in beta or random coil conformation, respectively.[7,11] Replacing the terminal PHE residue to cyclohexyl-L-alanine (CHA) lead to a full beta structure throughout the temperature range 4−25 °C.[11] CG simulations have been previously performed to investigate the self-assembly of bis(Ac-FLIVI)-K-K_4-CO-NH_2[7] and a BAPC consisted of bis(Ac-FLIVIGSII)-K-K_4-CO-NH_2 and bis(Ac-CHA-LIVIGSII)-K-K_4-CO-NH_2[8] using the MARTINI force field.[12] The results support that BAPs likely assemble into bilayer structures in BAPCs, and the two leaflets have minimal interdigitation. The coarse-grained simulations could not supply atomic level details of the backbone and side-chain interactions underlying the unusual stabilities of BAPCs. In this study, we exploit long-time molecular dynamics (MD) simulations at the atomistic level to examine the structure and organization of bilayers formed by three BAPs: bis(Ac-FLIVIGSII)-K-K_4-CO-NH_2, bis(Ac-CHA-LIVIGSII)-K-K_4-CO-NH_2, and bis(Ac-FLIVI)-K-K_4-CO-NH_2. A particular focus is to understand the nature of molecular interactions underlying the unusual thermal stability of BAPCs and the possible origins of thermally induced conformation transitions.

METHODS

MD Simulations. All simulations were performed using the GROMACS (Groningen Machine for Chemical Simulation) package version 4.0.5[13,14] in conjunction with the GROMOS 54A7 force field.[15] The solvent water was represented using the simple point charge (SPC) water model.[16] The solvent and solute were coupled independently to an external temperature bath (310 K) with a coupling constant of 0.1 ps using the Berendsen thermostat.[17] Periodic boundary conditions were imposed, and the pressure was maintained at 1 bar in the lateral and normal directions by weakly coupling to a semi-isotropic (for the simulations start from preassembled bilayer) or isotropic (for the simulations starting from randomized initial conformations) pressure bath. The isothermal compressibility was 4.5×10^{-5} bar^{-1}, and the coupling constant was 1 ps. The LINCS algorithm[18] was used to constrain the length of all covalent bonds within the solute, and the SETTLE algorithm[19] was used to constrain the geometry of the water molecules. Nonbonded interactions were evaluated using a twin-range method, where interactions within the short-range cutoff of 0.8 nm were calculated every step, and those interactions within the long-range cutoff of 1.4 nm were recalculated every three steps together with the pair list. To correct for the truncation of electrostatic interactions beyond the long-range cutoff, a reaction-field correction was applied using a relative dielectric permittivity of 78.[20] The mass of hydrogen atoms was increased to 4 amu by transferring mass from the atom to which it was attached, allowing a time step of 4 fs to be used to integrate the equations of motion. This mass redistribution damps high-frequency hydrogen-attached bond vibrations without changing the potential energy function or the thermodynamic properties of the system.[21−23]

System Setup. Three preassembled bilayers were generated for each BAP molecule (Figure 1). For this, the monomers were first constructed in fully extended configurations and then subjected to three independent 300 ns equilibrium simulations in water at 298 K. Three representative monomer structures were then taken from these simulations for each system that are relatively extended as observed in our previous CG simulations of BAPCs.[8] Each of the three selected monomer structures was then replicated on an 8 × 8 grid to generate a bilayer containing 128 BAP molecules. The distances between the BAP molecules in the same leaflet were such that the initial area per peptides was similar to value obtained in our previous CG simulations with the Martini force field (~1.4 nm^2).[8] The system was then solvated in a box of SPC water molecules and neutralized by adding an appropriate number of counterions (Na^+ and Cl^-) to a final salt concentration of 150 mM (Table 1). Each system was then minimized for 500 steps using a steepest-descent algorithm, followed by 50 ps of equilibration dynamics at 298 K in which the positions of the heavy atoms of BAP molecules were harmonically restrained using a force constant of 500 kJ mol^{-1} nm^2. All solvated bilayers were simulated for up to 1.1 μs (see Table 1) with all restraints removed, where the time evolution of the potential energy, area per lipid, and hydrogen-bonding pattern were monitored. In the third simulation of bis(Ac-FLIVIGSII)-K-K_4-CO-NH_2, defects in upper leaflets were observed during the early stage of the production run and persisted for the rest of the run. This is consistent with the expectation that the membrane resealing likely

Table 1. Summary of the Simulation Systems

hydrophobic segment	bis(Ac-FLIVIGSII)-	bis(Ac-CHA-LIVIGSII)-	bis(Ac-FLIVI)-	bis(Ac-FLIVI)-
initial configuration	bilayer	bilayer	bilayer	dispersed
initial box size (nm)	9.6 × 9.6 × 13.0	9.6 × 9.6 × 13.0	9.6 × 9.6 × 11.0	10.0 × 10.0 × 10.0
no. of atoms	~93000	~93000	~71000	~97000
simulation length[a] (μs)	1.1, 0. 96, 0.68	1.0, 0. 64, 0.70	1.0, 0.87, 0.96	0.25

[a]Each independent simulation was initiated from a different bilayer configuration.

DOI: 10.1021/acs.langmuir.6b02421
Langmuir 2016, 32, 9883−9891

requires a milliseconds time scale.[24] We repeated the simulation after an additional 80 ps restrained equilibration step at 273 K. No defects were observed in the new production run that followed. In addition to simulations initiated from preassembled bilayers, a separate simulation was performed to provide a primitive view of the early stages of the self-assembly process at atomistic level. For this, 16 bis(Ac-FLIVI)-K-K_4-CO-NH_2 molecules were randomly placed within a cubic water box of ∼10 nm in size. The peptides were initially separated at least 1.0 nm from one and another. The self-assembly simulation was performed for 250 ns (see Table 1).

Simulation Analysis. Unless stated otherwise, the structures of the bilayer were extracted from the last 400 ns trajectories every 0.1 ns for analysis. All analyses were performed for three independent simulations and then averaged. For analysis of the water residence time and hydrogen bond lifetime, structures extracted at 0.01 ns interval were used. Average hydrogen bond lifetimes were calculated from the last 100 ns trajectories. Care was taken to remove spurious, high-frequency transitions by removing all reversible transitions that occur within <0.02 ns. The area per peptide was computed as the lateral area of the simulation box divided by the number of peptides per leaflet. The 2D radii of gyration of BAP molecule in the bilayer plane (x−y plane) was calculated as the mass-weighted root-mean-square of the radii components on the x−y plane:

$$Rg_{(z)}{}^2 = \sum m_i r_i^2 / M \tag{1}$$

where r_i is the x−y components of the distance between atom i and the center of mass. The secondary structure was assigned using the STRIDE algorithm.[25] Structure clustering was performed with the GROMOS algorithm[26] based on the mutual backbone root-mean-square distance (RMSD) of the hydrophobic tails with a cutoff of 0.4, 0.4, and 0.2 nm for bis(Ac-FLIVIGSII)-K-K_4-CO-NH_2, bis(Ac-CHA-LIVIGSII)-K-K_4-CO-NH_2, and bis(Ac-FLIVI)-K-K_4-CO-NH_2, respectively.

The orientation of hydrophobic segments was characterized using the second-rank order parameter, defined as

$$P_2 = \frac{1}{2}(3\langle \cos^2 \theta \rangle - 1) \tag{2}$$

with θ being the angle between the bilayer normal and the vector from the carbonyl C to amide N of a specific residue. The square brackets denote the ensemble average. The cases of perfect parallel alignment, perfect antiparallel alignment, and completely random orientation with respect to the bilayer normal yield $P_2 = 1$, −0.5, and 0, respectively. To quantify the level of order in the packing of the side-chain phenyl group of PHE in bis(Ac-FLIVIGSII)-K-K_4-CO-NH_2 and bis(Ac-FLIVI)-K-K_4-CO-NH_2, a general order parameter was calculated as

$$S = \frac{4\pi}{5} \sum |\langle Y_2{}^m(\theta, \phi) \rangle|^2 \tag{3}$$

where $Y_2{}^m$ are second-rank spherical harmonics. The (θ, Φ) are the spherical polar coordinates of the unit vector normal to the phenyl ring. The average was performed over all phenyl rings and over all snapshots in the trajectories. S reflects the degree of alignment along a common vector and has a value of 1.0 for fully aligned system and 0 for fully random systems.

Peptide Synthesis, BAPC Formation, and Eosin Y Self-Quenching. Both peptides bis(Ac-FLIVIGSII)-K-K_4 and bis(Ac-FLIVI)-K-K_4 were synthesized as described previously[8,9,11] using solid phase peptide chemistry. They were dissolved individually into 2,2,2-trifluoroethanol, and absorbance of phenylalanine was taken to determine the concentration. In preparation for the formation of BAPCs, the peptides were combined in concentrations of 1 mM of each peptide and dried to remove the solvent. The dried peptides were hydrated in a dropwise fashion with 2.126 mM of either Eosin Y or Rhodamine 6G (both from Sigma-Aldrich, St. Louis, MO) final concentration at room temperature in distilled, deionized water or with 20, 50, 100, or 300 mM NaCl. After sitting for 30 min at room temperature, each solution was filtered through a 0.2 μm syringe-driven PTFE filter (EMD Millipore, Billerica, MA) and into Amicon Ultra-0.5 mL centrifugal cellulose filters with a 30 kDa molecular weight cutoff (EMD Millipore, Billerica, MA). BAPCs were centrifuged at 14000g using an Eppendorf 5415 D benchtop centrifuge to remove external dye from the BAPCs. Wash steps were performed using the same concentration of NaCl with which the BAPCs were formed, and they were centrifuged at 14000g; wash and the centrifugation steps were repeated until the externally bound dye was removed from the outer surface of the BAPCs. The filters were then inverted into clean collection tubes and centrifuged at 2000g to collect the washed BAPCs.

The harvested BAPCs from each salt concentration were then divided into two equal volumes for analysis. One half was brought up to a final concentration of 1 mM BAPCs in the equimolar salt solution in which they were prepared and washed. The other half was diluted to the same concentration in distilled, deionized water. The distilled, deionized water containing BAPCs was diluted as discussed previously in water and in 1 M NaCl. Fluorescence intensities for the encapsulated Eosin Y were measured using a CARY Eclipse fluorescence spectrophotometer (Varian Inc., Palo Alto, CA) immediately upon dilution using an excitation wavelength at 500 nm and observing the fluorescence from 505 to 800 nm within a 0.3 cm path length quartz cuvette (scan rate: 600 nm/min; PMT detector voltage: 600 V; excitation slit: 5 nm; emission slit: 5 nm). After the fluorescence was measured, the BAPCs from each salt concentration that were placed into water were then filtered through the Amicon Ultra-0.5 mL centrifugal cellulose filters as previously described to detect any contributing fluorescence from free Eosin in solution. The fluorescence of the filtrate was measured using the same procedure as used for the BAPCs.

RESULTS AND DISCUSSION

Structural Characteristics of BAP Bilayers. All three BAPs can maintain stable bilayer structures in all simulations starting from different initial conformations with proper equilibration. Key structural properties, e.g., bilayer thickness, number of hydrogen bonds, and area per peptides, were monitored during simulations to examine the level of convergence. As illustrated in Figure S1, virtually all structural properties reached a plateau within ∼300 ns and remain stable for the rest of simulations. As such, all analyses were performed using the last 400 ns of the trajectories. Key properties of the BAP bilayers are summarized in Table 2. As illustrated in Figure 2, the overall organization of BAP bilayers is very similar to those formed by phospholipids. The charged C-terminal poly lysine "headgroups" (blue) project toward bulk water, while the branched N-terminal hydrophobic residues (brown) pack together and form a hydrophobic core. For bis(Ac-FLIVIGSII)-K-K_4-CO-NH_2 and bis(Ac-CHA-LIVIGSII)-K-K_4-CO-NH_2, the hydrophilic residues (green) form an additional layer between the charged LYS residues and the hydrophobic layer. The average area per peptide is slightly larger (∼1.5 nm^2) for the BAPs with longer hydrophobic segments (bis(Ac-FLIVIGSII)-K-K_4-CO-NH_2 and bis(Ac-CHA-LIVIGSII)-K-K_4-CO-NH_2) than the 1.3 nm^2 observed with shorter hydrophobic segments (bis(Ac-FLIVI)-K-K_4-CO-NH_2 (Table 2)). The BAPs with longer tails also have larger 2D radii of gyration and form more tightly packed membranes than those with shorter hydrophobic branches (Table 2). Figure 3 shows the average electron density profiles of different components. The thickness of the bilayers, defined as the distance between the peaks of polylysine electron density profiles from the top and bottom leaflets (red traces in Figure 3), was ∼6 nm for bis(Ac-FLIVIGSII)-K-K_4-CO-NH_2 and bis(Ac-CHA-LIVIGSII)-K-K_4-CO-NH_2 and ∼5 nm for bis(Ac-FLIVI)-K-K_4-CO-NH_2. With all residues included, the electron density profile of either the top or the bottom leaflet (green traces in Figure 3) crosses the

DOI: 10.1021/acs.langmuir.6b02421
Langmuir 2016, 32, 9883−9891

Table 2. Key Structural and Dynamic Properties of BAP Bilayers[a]

hydrophobic segment	bis(Ac-FLIVIGSII)-	bis(Ac-CHA-LIVIGSII)-	bis(Ac-FLIVI)-
area per peptide (nm^2)	1.46 ± 0.13	1.51 ± 0.07	1.30 ± 0.03
$Rg(z)$ (nm)	0.63 ± 0.03	0.61 ± 0.04	0.53 ± 0.01
packing density[b]	0.85	0.78	0.68
S of PHE side chains	0.004 ± 0.001	N/A	0.02 ± 0.01
no. of intermolecular hydrogen bonds[c]	4.3 ± 0.3	4.0 ± 0.2	3.3 ± 0.5
no. of intramolecular hydrogen bonds[c]	6.7 ± 0.8	6.5 ± 0.8	4.4 ± 0.1
no. of BAP−water hydrogen bonds	9.7 ± 1.3	10.0 ± 1.1	3.2 ± 0.5
intermolecular hydrogen bond lifetime (ps)	371 ± 40	510 ± 130	1568 ± 871
intramolecular hydrogen bond lifetime (ps)	231 ± 20	219 ± 10	280 ± 36
no. of cross-leaflets hydrogen bonds	1.4 ± 0.1	1.8 ± 0.1	0.7 ± 0.3
cross-leaflets hydrogen bonds lifetime (ps)	525 ± 240	614 ± 153	282 ± 65
lowest water electron density (e nm^{-3})	5.2 ± 1.8	4.0 ± 1.0	3.7 ± 1.4
water conduct rate (nm^{-1} ns^{-1})	0.03 ± 0.02	0.03 ± 0.01	0.06 ± 0.01
av time for single water molecule cross the bilayer core (ns)	14 ± 6	17 ± 4	9 ± 1
peptide lateral diffusion coeff (10^{-10} cm^2/s)	2.1 ± 1.0	2.5 ± 0.7	2.3 ± 0.2

[a]All standard deviations shown were calculated from three independent runs performed for each BAP. [b]The packing density is defined as $\pi^*Rg(z)^2/A$, where A is the average area per peptide. [c]Only hydrogen bonds formed between hydrophobic segment were counted.

bilayer midplanes and penetrates into the other leaflet. The thickness of interdigitating regions was ∼2 nm, which is larger than those observed in phospholipid bilayer.[27]

Networks of Hydrophobic and Hydrogen-Bonding Interactions. A key objective of atomistic simulations has been to characterize the interactions among BAPs that give rise to the unusual stability of BAPCs. The substantial interdigitation in BAP bilayers appears to allow extensive interactions between the hydrophobic segments from two leaflets. As shown in Figure 3, interdigitated regions mainly include the N-terminal PHE1/CHA1 and LEU2 residues (blue and purple traces). In particular, the last PHE/CHA1 residue appears to play a dominant role in the interleaflet interactions, contributing over 80% of the penetrating part of the electron density profile. It was previously speculated that the aromatic side chains of PHE residues could form ordered structures with specific $\pi-\pi$ stacking as previously observed in peptide nanostructures.[28] However, the current simulations suggest that the phenyl rings bis(Ac-FLIVIGSII)-K-K_4-CO-NH_2 and bis(Ac-FLIVI)-K-K_4-CO-NH_2 bilayers are completely disordered, yielding diminishing general order parameters in both cases (see Table 2). The prediction that the aromatic nature of PHE side chains is not likely a key factor for the unusual stability of BAPCs is consistent with a previous study showing that replacing PHE with CHA does not significantly destabilized the BAPCS.[11] As shown in Figure 3B, PHE to CHA mutation does not reduce the level of leaflet interdigitation (Figure 2B, blue and purple trace). As detailed below, the substitution does slightly increase the level of disorder of BAP peptides in the bilayer and results in modest reduction in packing density and number of intra- and intermolecular interactions. The implication is that the bis(Ac-CHA-LIVIGSII)-K-K_4 bilayer should have slightly reduced (thermo)stability, which appears fully consistent with the previous experimental studies.[11]

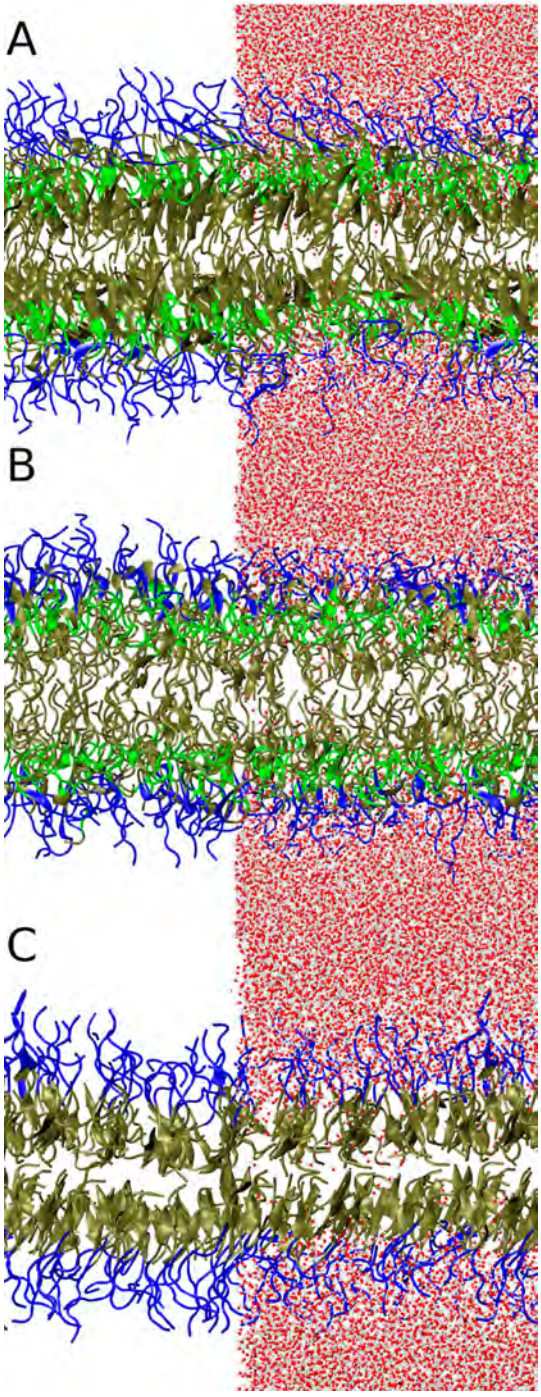

Figure 2. Representative structures of BAP bilayers, given as the last snapshot of simulation 1 for each system: (A) bis(Ac-FLIVIGSII)-K-K_4-CO-NH_2 (1.1 μs); (B) bis(Ac-CHA-LIVIGSII)-K-K_4-CO-NH_2 (1.0 μs), and (C) bis(Ac-FLIVI)-K-K_4-CO-NH_2 (1.0 μs). BAP molecules are shown in cartoon representations and colored according to the residue types (positive: blue; hydrophilic: green; hydrophobic: brown). Water molecules, represented as balls and sticks and colored according to atom type (O, red; H, white), are shown only for the right half for clarity.

DOI: 10.1021/acs.langmuir.6b02421
Langmuir 2016, 32, 9883−9891

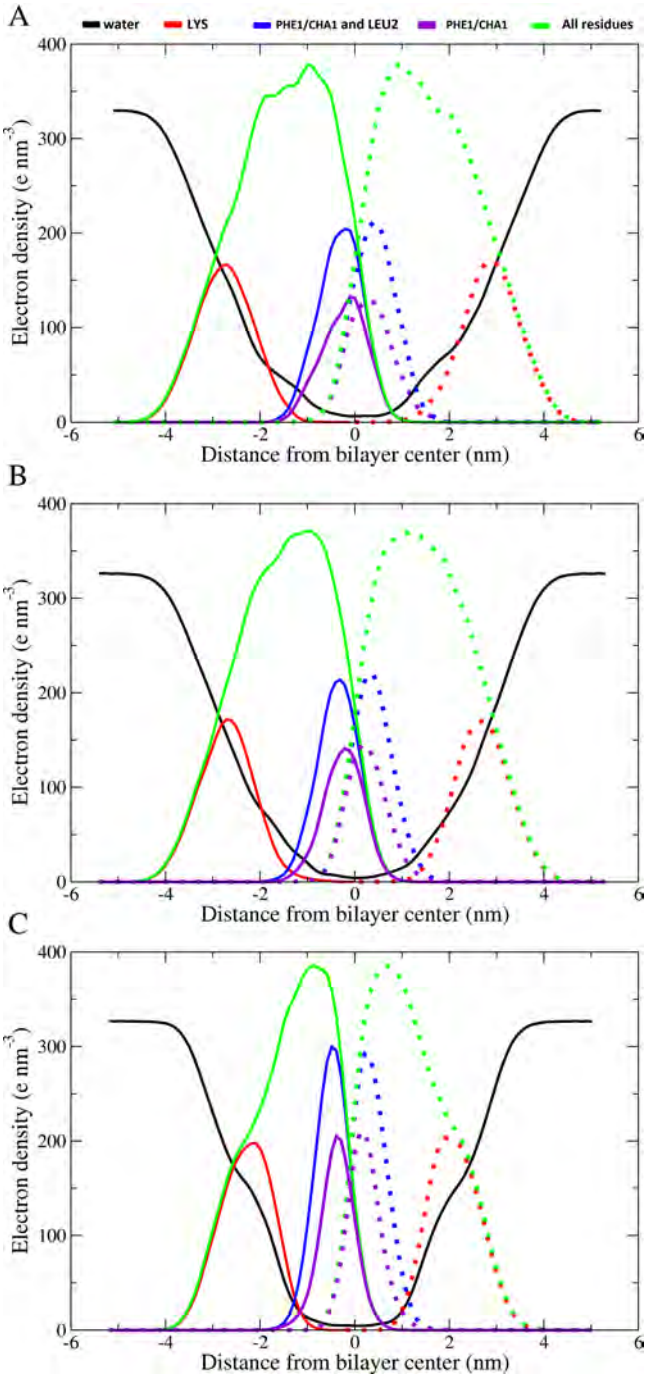

Figure 3. Electron density profiles of different components along the bilayer normal calculated from the last 400 ns of simulation trajectories: (A) bis(Ac-FLIVIGSII)-K-K_4-CO-NH_2; (B) bis(Ac-CHA-LIVIGSII)-K-K_4-CO-NH_2 and (C) bis(Ac-FLIVI)-K-K_4-CO-NH_2. The electron density profiles for residues in the top and bottom leaflets are shown in solid and dotted traces, respectively.

The interdigitation between leaflets allows extensive nonpolar interactions within and between leaflets, not only between terminal residues (PHE1 and LEU2) but also involving central hydrophobic residues (ILE3, VAL4, and ILE5). In particular, as illustrated in Figure S2, hydrophobic residues (ILE3: green; VAL4: orange; ILE5: brown) from the top leaflet can make close contacts with PHE1 from the bottom leaflet. Figure S3 shows the distribution of minimum distances between PHE1 side chains from one leaflet and to side chains of ILE3 (solid line), VAL4 (dashed line), and ILE5 (dotted line) from the other leaflet. These distributions clearly show peaks between 0.3 and 0.5 nm, which indicate the existence of close contacts. The population of PHE1/CHA1 involved in the interactions with these residues (minimum distance <0.5 nm) were similar in bis(Ac-FLIVIGSII)-K-K_4-CO-NH_2 (36%, 19%, and 12% for ILE3, VAL4, and ILE5, respectively) and bis(Ac-CHA-LIVIGSII)-K-K_4-CO-NH_2 (39%, 15%, and 10% for ILE3, VAL4, and ILE5, respectively). In bis(Ac-FLIVI)-K-K_4-CO-NH_2, the population of PHE1 involved in the cross-leaflets interactions is lower than the other two system (21%, 3%, and 3% for ILE3, VAL4, and ILE5, respectively), suggesting the packing of bis(Ac-FLIVI)-K-K_4-CO-NH_2 decreases the penetration of PHE1 into the opposite leaflet. The degree of interdigitation can be correlated with the strength of coupling between leaflets for phospholipid bilayers.[27] It is likely that substantial interdigitation in BAP bilayers, and thus stronger cross-leaflet hydrophobic interactions, is a key reason for the unusual stability of BAPCs.

Besides extensive hydrophobic interactions, BAP bilayers also support extensive backbone hydrogen-bonding interactions within and across leaflets that are completely absent in traditional phospholipid bilayers. On average, BAP molecules make 3.3−4.3 intermolecular hydrogen bonds, in addition to 4.4−6.7 intramolecular ones (i.e., between two hydrophobic branches) (see Table 2). Interdigitation also allows substantial cross-leaflet hydrogen-bonding interactions. The average number of cross-leaflet hydrogen bonds for each BAP molecule ranges from 0.7 to 1.8 for the three systems (Table 2). Importantly, the peptides do not appear to form stable and persisting β-sheets. The average lifetimes of these backbone hydrogen bonds are short, ranging only from ∼280 to ∼600 ps. The highly dynamic nature of the hydrogen-bonding network within the bilayers appears consistent with the ability of BAPCs to fuse or resize when assembled at room temperature. Nonetheless, the ability to form an extensive hydrogen-bonding network through the peptide backbone is clearly another key factor that contributes to BAPC stabilities. The ability to form hydrogen-bonding networks also greatly reduces the lateral diffusion constant of BAP molecules within the bilayers, which is about 1% of that of lipid molecules in more fluid phase membranes (Table 2).[29]

Conformational Properties of BAPs in the Bilayer. While the charged polylysine tails are highly disordered and well hydrated, the hydrophobic segments adopt more ordered structures to support extensive intra- and intermolecular hydrogen-bonding interactions (Figure 2). To examine the conformation of hydrophobic segment, cluster analysis based on the mutual backbone RMSD was performed. The centroid structures of the first five clusters are shown in Figure 4. The first cluster accounts for approximately 60%−69% of the ensemble, where both hydrophobic segments are relatively extended conformation. For bis(Ac-FLIVIGSII)-K-K_4-CO-NH_2 and bis(Ac-CHA-LIVIGSII)-K-K_4-CO-NH_2, hydrophobic segments can be substantially disordered in clusters 2−5, which together account for ∼25% of the population. In shorter bis(Ac-FLIVI)-K-K_4-CO-NH_2, the hydrophobic segments adopt the extended structure in the top four clusters. Interestingly, the longer BAP peptides with more disordered conformations also have shorter intermolecular hydrogen bond lifetime (<600 ps) compared to the shorter bis(Ac-FLIVI)-K-K_4-CO-NH_2 peptides (>1000 ps) (see Table 2). A reduced

DOI: 10.1021/acs.langmuir.6b02421
Langmuir 2016, 32, 9883−9891

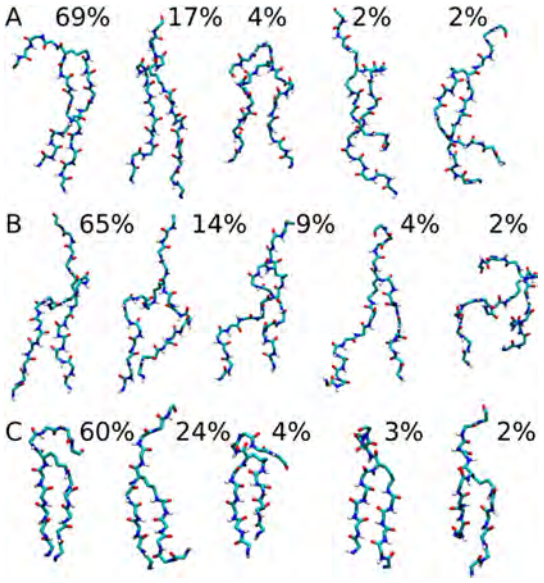

Figure 4. Centroid structures of the five most populated clusters of BAP conformations in bilayers: (A) bis(Ac-FLIVIGSII)-K-K_4-CO-NH_2, (B) bis(Ac-CHA-LIVIGSII)-K-K_4-CO-NH_2, and (C) bis(Ac-FLIVI)-K-K_4-CO-NH_2. The clustering was performed based on mutual backbone RMSD of the hydrophobic tails with a cutoff of 0.4, 0.4, and 0.2 nm for the above three systems, respectively.

intrahydrogen bond lifetime was also observed in more disordered CHA-mutation bilayers (~220 ps).

The average secondary structure of BAP was calculated from last 400 ns of simulations. The results, summarized in Figure 5, show that BAPs mainly sample beta and coil-like secondary structures in the bilayer. This is consistent with previous CD studies on BAPCs freshly assembled at the room temperature.[11] Replacing PHE with CHA leads to substantial decrease in the level of β secondary structure in the hydrophobic segment, even though the average numbers of intra- and interpeptide hydrogen bonds remain very similar (see Table 2). For bis(Ac-FLIVIGSII)-K-K_4-CO-NH_2 and bis(Ac-CHA-LIVIGSII)-K-K_4-CO-NH_2, transient helices involving SER7 to ILE9 (on the main branch) and polylysine residues have been observed in the bilayers. This appears to reflect an intrinsic conformational tendency of BAPs. Similar helical propensities can be observed for BAP monomers in water (Figure S4), even though the random coil propensity is higher compared to when incorporated into bilayers. In Figure 6, we further examine the ordering of BAP peptides with respect to the bilayer

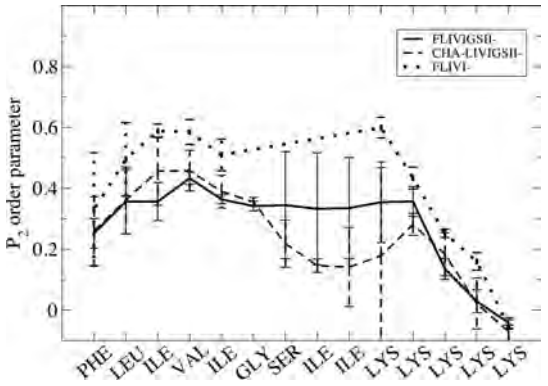

Figure 6. P_2 order parameter as a function of the sequence. Data were collected from last 400 ns of simulations and were averaged over both tails. The error bars were calculated as the standard deviations from the three independent runs performed for each BAP.

normal, as quantified by the second rank order parameter P_2 as a function of residue number. The results correlate well with the peptide secondary structures discussed above. All three BAPs bilayer had similar, diminishing order parameters in the polylysine headgroup region but demonstrate varied levels of ordering in the hydrophobic branches. The shorter BAP, bis(Ac-FLIVI)-K-K_4-CO-NH_2, prefers more extended structures (Figure 4) and has the most ordered hydrophobic region among all three sequences.

Peptide–Water Interactions in BAP Bilayers. Another distinct property of BAP bilayers involves the extent and nature of peptide–water interactions. In phospholipid bilayers, there is essentially no water density in the hydrophobic center.[30] For BAP bilayers, the water density drops from ~320 e nm^{-3} (bulk water region) to ~40 e nm^{-3} after crossing the polylysine head region but remains nondiminishing throughout the BAP bilayers, with the lowest water electron density of ~3–5 e nm^{-3} near the bilayer center (see Figure 3, black traces, and Table 2). The average electron density of water in the hydrophobic core region was 4–8 e nm^{-3}. As a result, each BAP molecule can form ~3–10 water–backbone hydrogen bond interactions in the hydrophobic region (Table 2). Importantly, water molecules in the hydrophobic regions of BAP bilayers are highly dynamic. The average water residence time within the bilayer hydrophobic core is only ~0.2 ns, with only a few "structural" water molecules that have long residence times up to ~40 ns. The average rate of water transport is ~0.03 nm^{-1} ns^{-1} for BAP bilayers with longer hydrophobic

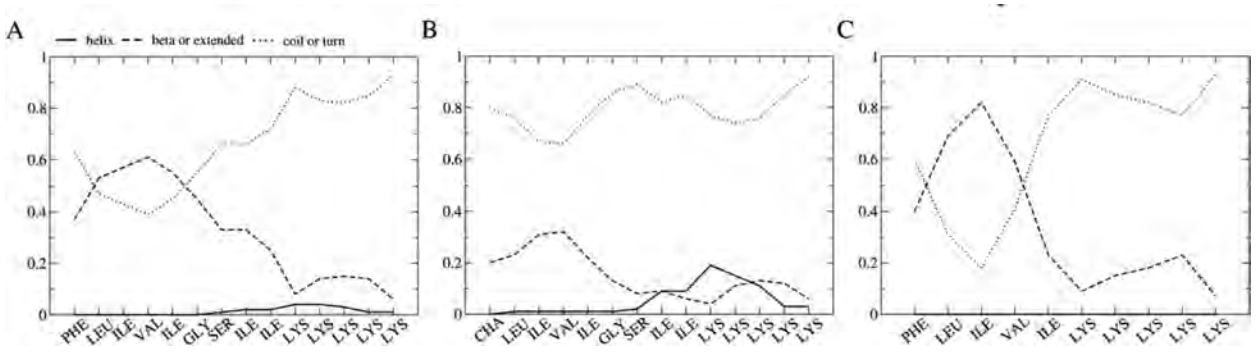

Figure 5. Secondary structures of BAPs in the bilayer: (A) bis(Ac-FLIVIGSII)-K-K_4-CO-NH_2, (B) bis(Ac-CHA-LIVIGSII)-K-K4v, and (C) bis(Ac-FLIVI)-K-K_4-CO-NH_2. Data were collected from last 400 ns of simulations and averaged over both branched hydrophobic segments.

DOI: 10.1021/acs.langmuir.6b02421
Langmuir 2016, 32, 9883–9891

segments and ~0.06 nm^{-1} ns^{-1} for the BAP bilayer with short hydrophobic segments. The average time for a single water molecule to cross the bilayer core is 9−17 ns (Table 2). Figure S5 shows a typical trajectory of water diffusion spontaneously through the BAP bilayer. Note that although water can penetrate easily into the BAP bilayer, no density of ions was observed in the bilayer core, suggesting that ions could not permeate spontaneously through BAP bilayers. Water permeability may also contribute to the unusual stability of BAPCs, allowing BAPCs to expand or contract in response to changing external osmotic pressure.

Change of BAPC Internal Solute Concentration in Response to Salt Gradient. To test the selective permeation of water across BAP bilayers in the absence of ions, we examined the effects of dilution on the internal solute concentration when BAPCs were placed in external solutions with different salt concentrations. This was achieved by measuring the fluorescence intensity of two self-quenching dyes Eosin Y—a negatively charged dye—and Rhodamin 6G—a positively charged dye—encapsulated within the BAPCs (see Figure S6).[11] If the BAP bilayer is semipermeable to water, the flux of water in to or out of the dye-filled capsules will change the internal concentration of the dyes and lead to changes in the fluorescence intensity. To normalize for batch to batch variations with dye encapsulation from different experiments, we only examine the relative fluorescence intensity change when diluted in hyper- or hypotonic solutions with respect to the reference BAPCs that were diluted into isotonic solutions (see Methods section for details). The measured fluorescence intensity was further corrected to account for different fluorescence properties of both Eosin Y and Rhodamine 6G dyes in water versus NaCl solutions.

The results, summarized in Figure 7, clearly support the prediction that BAP bilayers are permeable to water but not to ions. Exposure of water-filled BAPCs (that is, zero internal NaCl concentration) to 1.0 M NaCl buffer leads to ~14% decrease in internal Eosin Y fluorescence intensity and ~8% decrease in internal Rhodamin 6G fluorescence intensity (leftmost bars), suggesting a net out flux of water and thus increase in internal dye concentration. In contrast, when BAPCs prepared with different internal NaCl concentrations were placed in pure water, there were net increases in both the Eosin Y and Rhodamine 6G fluorescence intensities (right four sets of bars of Figure 7). The degree of fluorescence intensity increase clearly correlates with the NaCl concentration difference across the BAP bilayer. Assuming that there is minimal ion movement across BAP bilayers, we can further quantify the Eosin Y concentration changes using a standard curve of fluorescence intensity. The results are summarized in Figure S4. Exposing BAPCs with initial NaCl concentration of 300 mM to pure water dilutes the internal Eosin Y concentration to approximately 500 μM, compared to the initial concentration of 2130 μM where the BAPCs were formed. In contrast, exposing BAPCs with no internal salt to 1.0 M NaCl buffer approximately doubles the internal Eosin Y concentration. Upon filtering the BAPCs from these solutions (see Methods section), the fluorescence emission spectra measured were similar to that of pure water. This shows that the fluorescence seen in these experiments are due to encapsulated dye and not free dye, further supporting the idea that BAPCs remain intact while changing salt concentrations. We note that all BAPCs were filled with the same concentration of dyes; fusion between BAPCs should not lead to any change in fluorescence. Together, these experiments reveal a surprising level of plasticity and stability associated with BAP bilayers under osmotic pressure. The structural basis of such plasticity is not obvious from the current simulations and will be further investigated in future studies.

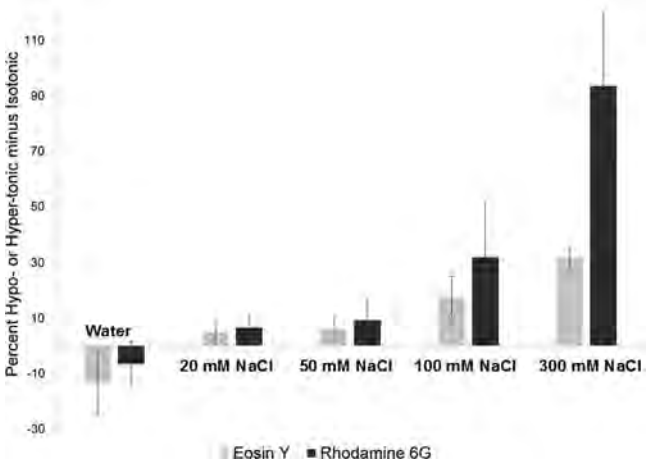

Figure 7. Intensity differences between the percent fluorescence seen of Eosin Y and Rhodamine 6G dyes encapsulated within BAPCs made in increasing concentrations of salt. The horizontal axis labels show the salt concentration, which was encapsulated within the BAPCs along with the respective dye. The vertical axis represents the difference in percent between the fluorescence seen in hyper- or hypotonic solutions minus that fluorescence seen in isotonic solutions. The discrepancy seen between the two dyes in 300 mM salt may be due to large fluorescence changes seen with Rhodamine 6G in salt solutions. Error bars represent standard error of the mean with $n \geq 3$.

Early Stages of Aggregation and Self-Assembly of BAPs. Besides simulations initiated from preformed bilayers, a separate simulation was performed examine the early stages of BAP aggregation and self-assembly at the atomistic level. The simulation was initiated from 16 bis(Ac-FLIVI)-K-K_4-CO-NH_2 peptides randomly placed as monomers in a water box. As shown in Figure 8, small clusters emerged quickly, within 80 ns (Figure 8B), which merged into a single cluster by 250 ns (Figure 8C). The large cluster has a connected hydrophobic core region (Figure 8C, brown) with the LYS residues projecting outward (Figure 8C, blue). In the initial cluster, the terminal PHE1 residue (van der Waals surface) tended to stack together (Figure 8B,C), thereby restricting the relative orientation of neighboring BAP peptides. As a result, the peptides tend to adopt parallel orientation or tail-to-tail orientation. For example, Figure 8D shows the snapshot of a cluster containing six BAP molecules observed at ~80 ns, in which all peptides have a neighbor peptide adopted either parallel or tail-to-tail orientation.

We note that another vesicle-forming peptide, self-assembling peptide 2 (SA2 peptide, Ac-AAVVLLLWEE-COOH), was recently shown to adopt antiparallel and interdigitated structures.[31] Increasing the GLU residues at the C-terminus of SA2 from 2 to 7 did not change the overall structure of SA2 vesicle.[32,33] Thus, the difference in the peptide orientation in SA2 and BAP assemblies is not likely due to different head−tail ratios and is more likely a result of the peptide sequences.[32] As shown in the self-assembly simulation of BAP, the PHE/CHA clusters formed during the early stages of aggregation would make a parallel/tail-to-tail orientation more favored. As the

DOI: 10.1021/acs.langmuir.6b02421
Langmuir 2016, 32, 9883−9891

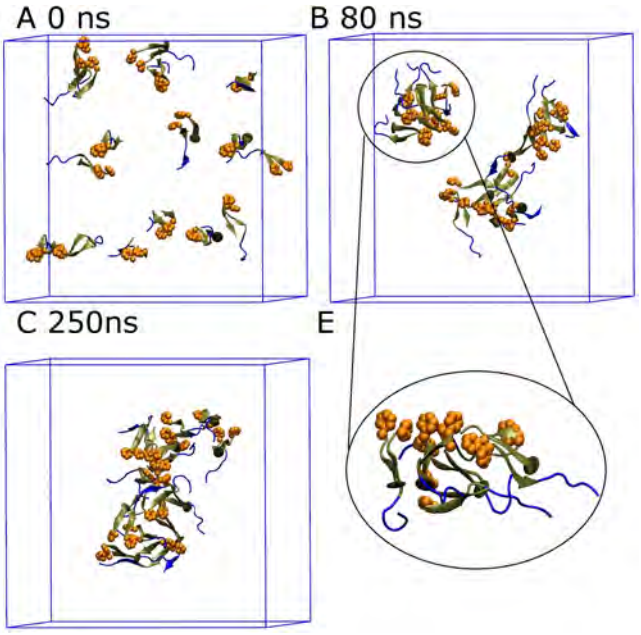

Figure 8. Snapshots from early stages of BAP aggregation and self-assembly at (A) 0, (B) 80, and (C) 250 ns. (D) Close-up view of cluster 1 at 80 ns. BAP molecules are shown in cartoon representations and colored according to residue types (positive: blue; hydrophilic: green; hydrophobic: brown). PHE1 residues are represented using van der Waals surfaces and colored in orange.

PHE cluster kept growing during the assembling of small clusters, the preference of parallel orientation may be preserved in the final vesicle structure.

CONCLUSIONS

Long-time scale atomistic simulations have been performed to analyze the structure and interactions of three different BAP bilayers. The results support that the overall structure of BAP bilayers is similar to those formed by phospholipids. However, BAP bilayers contain extensive networks of intra- and intermolecular backbone hydrogen-bonding interactions. BAP bilayers also possess a larger degree of interdigitation between the top and bottom leaflets. The interdigitation region is dominated by the interactions between last two residues, which forms early in the assembly process and plays an important role in the ultimate peptides alignment as well as maintaining bilayer stability. In addition, water was found able to readily permeate through the BAP bilayers while ions cannot, a prediction that has been subsequently validated by fluorescence measurements of encapsulated self-quenching Eosin Y. Together, the current atomistic simulations and experiment yield important new details on the molecular interactions underlying the unusual stability of BAPCs and provide a foundation for future efforts that aim to rationally modify the BAP sequence to improve the properties of BAPCs as a new class of delivery vehicle.

ASSOCIATED CONTENT

Supporting Information

The Supporting Information is available free of charge on the ACS Publications website at DOI: 10.1021/acs.langmuir.6b02421.

Figures S1−S6 (PDF)

AUTHOR INFORMATION

Corresponding Author

*Phone (785) 532-2518; Fax (785) 532-7278; e-mail jianhanc@ksu.edu (J.C.).

Notes

The authors declare no competing financial interest.

ACKNOWLEDGMENTS

This work was supported by the National Science Foundation (CHE 1265850 to J.C.) and National Institutes of Health (GM114300 to J.C.). Part of the computing for this project was performed on the Beocat Research Cluster at Kansas State University. Computer resources were also used at Extreme Science and Engineering Discovery Environment (XSEDE) facilities (TG-MCB140210). This work is contribution number 16-324-J from the Kansas Agricultural Experiment Station.

REFERENCES

(1) Allen, T. M.; Cullis, P. R. Drug delivery systems: Entering the mainstream. *Science* **2004**, *303* (5665), 1818−1822.
(2) Torchilin, V. P.; Lukyanov, A. N. Peptide and protein drug delivery to and into tumors: challenges and solutions. *Drug Discovery Today* **2003**, *8* (6), 259−266.
(3) Muller, R. H.; Keck, C. M. Challenges and solutions for the delivery of biotech drugs − a review of drug nanocrystal technology and lipid nanoparticles. *J. Biotechnol.* **2004**, *113* (1−3), 151−170.
(4) Reischl, D.; Zimmer, A. Drug delivery of siRNA therapeutics: potentials and limits of nanosystems. *Nanomedicine* **2009**, *5* (1), 8−20.
(5) Torchilin, V. P. Recent approaches to intracellular delivery of drugs and DNA and organelle targeting. *Annu. Rev. Biomed. Eng.* **2006**, *8* (1), 343−375.
(6) Frokjaer, S.; Otzen, D. E. Protein drug stability: a formulation challenge. *Nat. Rev. Drug Discovery* **2005**, *4* (4), 298−306.
(7) Gudlur, S.; Sukthankar, P.; Gao, J.; Avila, L. A.; Hiromasa, Y.; Chen, J.; Iwamoto, T.; Tomich, J. M. Peptide nanovesicles formed by the self-assembly of branched amphiphilic peptides. *PLoS One* **2012**, *7* (9), e45374.
(8) Sukthankar, P.; Gudlur, S.; Avila, L. A.; Whitaker, S. K.; Katz, B. B.; Hiromasa, Y.; Gao, J.; Thapa, P.; Moore, D.; Iwamoto, T.; Chen, J.; Tomich, J. M. Branched oligopeptides form nanocapsules with lipid vesicle characteristics. *Langmuir* **2013**, *29* (47), 14648−14654.
(9) Sukthankar, P.; Avila, L. A.; Whitaker, S. K.; Iwamoto, T.; Morgenstern, A.; Apostolidis, C.; Liu, K.; Hanzlik, R. P.; Dadachova, E.; Tomich, J. M. Branched amphiphilic peptide capsules: Cellular uptake and retention of encapsulated solutes. *Biochim. Biophys. Acta, Biomembr.* **2014**, *1838* (9), 2296−2305.
(10) Avila, L. A.; Aps, L. R. M. M.; Sukthankar, P.; Ploscariu, N.; Gudlur, S.; Šimo, L.; Szoszkiewicz, R.; Park, Y.; Lee, S. Y.; Iwamoto, T.; Ferreira, L. C. S.; Tomich, J. M. Branched Amphiphilic Cationic oligopeptides form peptiplexes with DNA: A study of their biophysical properties and transfection efficiency. *Mol. Pharmaceutics* **2015**, *12* (3), 706−715.
(11) Sukthankar, P.; Whitaker, S. K.; Garcia, M.; Herrera, A.; Boatwright, M.; Prakash, O.; Tomich, J. M. Thermally induced conformational transitions in nascent Branched Amphiphilic Peptide Capsules. *Langmuir* **2015**, *31* (10), 2946−2955.
(12) Monticelli, L.; Kandasamy, S. K.; Periole, X.; Larson, R. G.; Tieleman, D. P.; Marrink, S. J. The MARTINI coarse-grained force field: Extension to proteins. *J. Chem. Theory Comput.* **2008**, *4* (5), 819−834.
(13) Hess, B.; Kutzner, C.; van der Spoel, D.; Lindahl, E. GROMACS 4: algorithms for highly efficient, load-balanced, and scalable molecular simulation. *J. Chem. Theory Comput.* **2008**, *4* (3), 435−447.
(14) van der Spoel, D.; Lindahl, E.; Hess, B.; Groenhof, G.; Mark, A. E.; Berendsen, H. J. C. GROMACS: fast, flexible, and free. *J. Comput. Chem.* **2005**, *26* (16), 1701−1718.

DOI: 10.1021/acs.langmuir.6b02421
Langmuir 2016, 32, 9883−9891

(15) Schmid, N.; Eichenberger, A. P.; Choutko, A.; Riniker, S.; Winger, M.; Mark, A. E.; van Gunsteren, W. F. Definition and testing of the GROMOS force-field versions 54A7 and 54B7. *Eur. Biophys. J.* **2011**, *40* (7), 843−856.
(16) Berendsen, H. J. C.; Postma, J. P. M.; van Gunsteren, W. F.; Hermans, J. Interaction models for water in relation to protein hydration. In *Intermolecular Forces*; Pullman, B., Ed.; Reidel: Dordrecht, 1981; pp 331−342.
(17) Berendsen, H. J. C.; Postma, J. P. M.; van Gunsteren, W. F.; DiNola, A.; Haak, J. R. Molecular dynamics with coupling to an external bath. *J. Chem. Phys.* **1984**, *81*, 3684.
(18) Hess, B.; Bekker, H.; Berendsen, H. J. C.; Fraaije, J. G. E. M. LINCS: a linear constraint solver for molecular simulations. *J. Comput. Chem.* **1997**, *18* (12), 1463−1472.
(19) Miyamoto, S.; Kollman, P. A. SETTLE: an analytical version of the SHAKE and RATTLE algorithm for rigid water models. *J. Comput. Chem.* **1992**, *13* (8), 952−962.
(20) Tironi, I. G.; Sperb, R.; Smith, P. E.; van Gunsteren, W. F. A generalized reaction field method for molecular dynamics simulations. *J. Chem. Phys.* **1995**, *102*, 5451.
(21) Feenstra, K. A.; Hess, B.; Berendsen, H. J. C. Improving efficiency of large time-scale molecular dynamics simulations of hydrogen-rich systems. *J. Comput. Chem.* **1999**, *20* (8), 786−798.
(22) Jia, Z.; O'Mara, M. L.; Zuegg, J.; Cooper, M. A.; Mark, A. E. The effect of environment on the recognition and binding of vancomycin to native and resistant forms of lipid II. *Biophys. J.* **2011**, *101* (11), 2684−2692.
(23) Anézo, C.; de Vries, A. H.; Höltje, H.-D.; Tieleman, D. P.; Marrink, S.-J. Methodological issues in lipid bilayer simulations. *J. Phys. Chem. B* **2003**, *107* (35), 9424−9433.
(24) Hibino, M.; Itoh, H.; Kinosita, K. Time courses of cell electroporation as revealed by submicrosecond imaging of transmembrane potential. *Biophys. J.* **1993**, *64* (6), 1789−1800.
(25) Frishman, D.; Argos, P. Knowledge-based protein secondary structure assignment. *Proteins: Struct., Funct., Genet.* **1995**, *23* (4), 566−579.
(26) Daura, X.; Antes, I.; van Gunsteren, W. F.; Thiel, W.; Mark, A. E. The effect of motional averaging on the calculation of NMR-derived structural properties. *Proteins: Struct., Funct., Genet.* **1999**, *36* (4), 542−555.
(27) Chiantia, S.; London, E. Acyl chain length and saturation modulate interleaflet coupling in asymmetric bilayers: Effects on dynamics and structural order. *Biophys. J.* **2012**, *103* (11), 2311−2319.
(28) Sukthankar, P.; Gudlur, S.; Avila, L. A.; Whitaker, S. K.; Katz, B. B.; Hiromasa, Y.; Gao, J.; Thapa, P.; Moore, D.; Iwamoto, T.; Chen, J.; Tomich, J. M. Branched oligopeptides form nanocapsules with lipid vesicle characteristics. *Langmuir* **2013**, *29* (47), 14648−54.
(29) Poger, D.; Mark, A. E. Lipid bilayers: The effect of force field on ordering and dynamics. *J. Chem. Theory Comput.* **2012**, *8* (11), 4807−4817.
(30) Poger, D.; van Gunsteren, W. F.; Mark, A. E. A new force field for simulating phosphatidylcholine bilayers. *J. Comput. Chem.* **2010**, *31* (6), 1117−1125.
(31) Rad-Malekshahi, M.; Visscher, K. M.; Rodrigues, J. P. G. L. M.; de Vries, R.; Hennink, W. E.; Baldus, M.; Bonvin, A. M. J. J.; Mastrobattista, E.; Weingarth, M. The supramolecular organization of a peptide-based nanocarrier at high molecular detail. *J. Am. Chem. Soc.* **2015**, *137* (24), 7775−7784.
(32) Rad-Malekshahi, M.; Lempsink, L.; Amidi, M.; Hennink, W. E.; Mastrobattista, E. Biomedical applications of self-assembling peptides. *Bioconjugate Chem.* **2016**, *27* (1), 3−18.
(33) van Hell, A. J.; Costa, C. I. C. A.; Flesch, F. M.; Sutter, M.; Jiskoot, W.; Crommelin, D. J. A.; Hennink, W. E.; Mastrobattista, E. Self-Assembly of recombinant amphiphilic oligopeptides into vesicles. *Biomacromolecules* **2007**, *8* (9), 2753−2761.

DOI: 10.1021/acs.langmuir.6b02421
Langmuir 2016, 32, 9883−9891